RESEARCH ARTICLE | MARCH 13 2025

Analyzing electrical transport phenomena in $NdMn_{0.3}Co_{0.7}O_3$

Special Collection: 16th Joint MMM-Intermag Conference

Farooq Hussain Bhat ; Jan Asifa; Ghazala Anjum

AIP Advances 15, 035323 (2025)
https://doi.org/10.1063/9.0000919

Analyzing electrical transport phenomena in $NdMn_{0.3}Co_{0.7}O_3$

Cite as: AIP Advances 15, 035323 (2025); doi: 10.1063/9.0000919
Submitted: 11 November 2024 • Accepted: 10 February 2025 •
Published Online: 13 March 2025

Farooq Hussain Bhat,[1,a)] Jan Asifa,[1] and Ghazala Anjum[2]

AFFILIATIONS

[1] Department of Physics, Islamic University of Science and Technology, Kashmir, Awantipora, J&K, India
[2] Department of Physics, Government SAM Degree College, Budgam, J&K, India

Note: This paper was presented at the 16th Joint MMM-Intermag Conference.
[a)]**Author to whom correspondence should be addressed:** fhbhat@gmail.com

ABSTRACT

The effect of Co doping on the conduction mechanism of polycrystalline $NdMn_{0.3}Co_{0.7}O_3$ (NMCO7) sample, is studied by measuring the temperature-dependent dc resistivity ρ (T) from 150 K to 400 K. The temperature dependence of electrical resistivity indicates a typical semiconducting behavior of NMCO7. The electrical resistivity data as a function of temperature is fitted using models such as the Arrhenius law, small polaron hopping, and Mott-variable range hopping. The data follows the thermal activation and the small polaron hopping model in the high-temperature region, the latter account for electron–phonon interaction. In contrast, at lower temperatures, the Mott-VRH yield better results. Hence, in the NMCO7 system, the charge transport properties are governed by a complex interplay among thermal activation localized electronic states, and Coulomb interactions.

I. INTRODUCTION

$AMnO_3$-type manganites have attracted considerable research attention over the last few decades due to their diverse physical properties, which arise from the interplay between lattice, orbital, and spin degrees of freedom. Many researchers have focused on investigating their potential for various technological applications, including magnetic sensors, read heads, magnetic data storage, infrared detectors, and other spintronic devices.[1] In rare-earth manganites, $RMnO_3$ (R is a rare-earth element), the transition metal ions and their oxidation states are pivotal in determining the material's electrical and magnetic properties.[2,3] For instance, in $LaMnO_3$, doping with Co or Ca, Sr, and Pb at the Mn site or the La site respectively induces mixed valency in Mn i.e., Mn^{3+} and Mn^{4+}.[4,5] This mixed valency facilitates rapid electron hopping between Mn^{3+} and Mn^{4+} via the double-exchange (DE) mechanism, imparting ferromagnetic character to the ground state and the other key electrical properties. The DE mechanism is dependent on the Mn–O bond lengths and Mn–O–Mn bond angle.[6,7] The modification of structural, transport, and magnetic properties in perovskite manganites has also been achieved through doping with other cations.[6,8,9]

$NdMnO_3$ is a fascinating rare-earth manganite that exhibits ferromagnetic ordering within the Nd sublattice at T_l = 20 K and A-type antiferromagnetic ordering of Mn ions at T_N = 82 K, where T_N represent the Néel temperature.[10–12] The Mn^{3+}/Mn^{4+} ratio significantly contributes to the complexity and uniqueness of the transport and magnetic properties in Nd-based manganites,[13,14] distinguishing them from La-based manganites.[15]

Wang *et al.* have extensively studied the electrical transport properties etc. of $NdMnO_3$ and other manganites.[2,3,16–19] They explained electrical transport properties of $NdMnO_3$ using thermal activation model and a weak magnetoresistance of ~8% under a 6 T magnetic field.[16] In a different study on $Nd_{1-x}Sr_xMnO_3$ ($0.2 \leq x \leq 0.5$) the complex magnetic behavior was attributed to the competition between double-exchange (dominating below T_C) and polarons (significant above T_C).[2] Related studies on $SrMnO_3$ report significant magnetoresistance (16.68%) under a 6 T field near room temperature,[17,18] while $La_{1-x}Ba_xMnO_3$ shows a Griffiths phase and large magnetoresistance (~44.7%) at room temperature under a 6 T field, highlighting the potential of manganites for MR device applications.[19]

We carried out temperature-dependent resistivity measurements of $NdMnO_3$ doped with 70% Co ($NdMn_{0.3}Co_{0.7}O_3$) to

examine its electrical properties. The resistivity data was analyzed using thermal activation, small polaron hopping (SPH), and variable range hopping (VRH) models.

II. EXPERIMENT

The single-phase $NdMn_{0.3}Co_{0.7}O_3$ (NMCO7), (the x-ray diffraction spectrum is reported somewhere else[20]) sample was synthesized using a solid-state reaction method. High-purity oxides (Nd_2O_3, MnO_2, and Co_3O_4) were combined in stoichiometric ratios and thoroughly ground with an agate mortar to achieve a homogeneous mixture. After the mixture was calcined, it sintered at 900 °C for ~20 h. The sintered powder was then pressed into pellets with a diameter of 10 mm and subjected to a second sintering at 1150 °C for 24 h. The resistivity versus temperature measurements were conducted utilizing resistivity measurement set up at UGC DAE, Indore.

III. RESULTS AND DISCUSSIONS

A. Transport studies

The variation of resistivity with temperature for the NMCO7 sample from 150 K to 400 K is shown in Fig. 1. The figure depicts a decrease in the sample's resistivity with increasing temperature, demonstrating typical semiconducting behavior. Mixed valence manganites exhibit a complicated transport mechanism that can be characterized by several models, including the thermal activation model or bandgap model, SPH, and VRH. Certain perovskites can exhibit all three mechanisms across different temperature ranges.[21,22] These models offer a valuable theoretical framework for understanding the electrical transport behavior of perovskite semiconductor materials, capturing the intricate electronic dynamics involved in these materials.

TABLE I. Fit parameters for NMCO7 sample calculated using thermal activation and SPH model.

Sample	E_a (eV)	E_p (eV)	$\frac{\theta_p}{2}$ (K)	ν_{ph} (Hz)	γ_p	$\frac{I}{\varphi}$
NMCO7	0.2108	0.238 579	265.67	1.107×10^{13}	10.422	0.880

To study the conduction mechanism in the NMCO7 sample, we fitted the experimental resistivity data with the above mentioned models. In the high-temperature regime, the data follows thermal activation and the SPH model. The thermal activation model suggests that carriers in perovskite semiconductors must acquire sufficient thermal energy to surpass the lattice potential barrier, thereby enabling transport within the crystal.[16] In these scenarios, the resistivity adheres to the Boltzmann law, which is expressed as follows:

$$\rho = \rho_0 e^{\frac{E_a}{K_B T}} \quad (1)$$

Here ρ_o represents a pre-exponential factor, E_a denotes the activation energy, and K_B is the Boltzmann constant. The E_a for the NMCO7 sample (as shown in Table I) is obtained from the slope of lnρ versus 1/T graph presented in Fig. 2(a).

The Boltzmann law, commonly used to describe thermally activated transport, does not account for the influence of electron–phonon (e-ph) interactions. Therefore, to delve deeper into the mechanism of hopping conduction and evaluate the strength of the e-ph interaction, we used the SPH model established by Mott

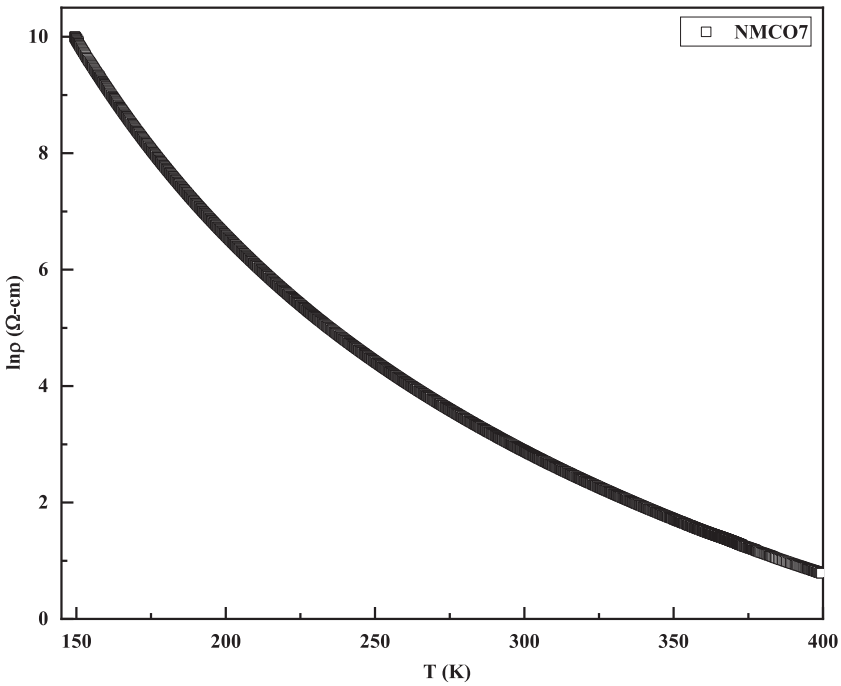

FIG. 1. Temperature-dependent resistivity of NMCO7.

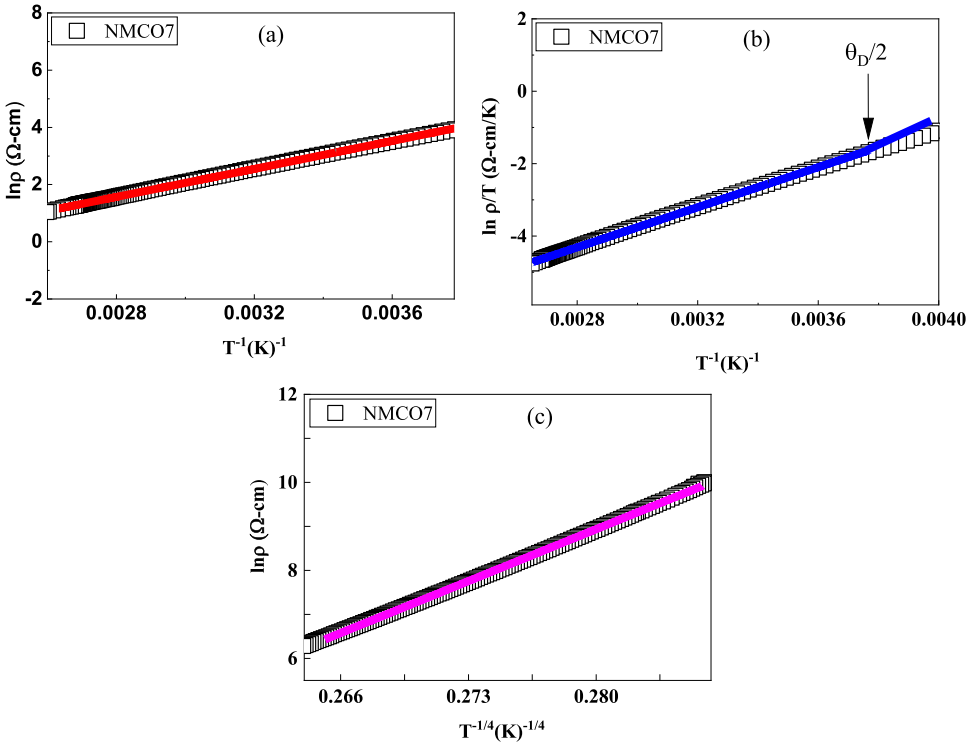

FIG. 2. Plots of (a) ln ρ vs T^{-1} (b) ln ρ/T vs T^{-1} (c) ln ρ vs $T^{-1/4}$ for NMCO7 fitted using thermal activation, SPH, and Mott-VRH respectively.

and Davis[23] to fit the temperature-dependent resistivity data. Furthermore, it has been established that, in rare-earth transition metal oxide systems, high-temperature transport is predominantly governed by the thermally activated hopping of small polarons.[23] The SPH model describes the coupling of electrons or holes in the perovskite semiconductor with the polarization field induced by lattice distortions, resulting in the formation of a quasi-particle known as the small polaron.[16] Based on this model, the expression for electrical resistivity can be represented as follows:[23–25]

$$\frac{\rho}{T} = \rho_0 e^{\frac{E_p}{K_B T}} \tag{2}$$

Where ρ_o represents a pre-exponential factor, E_p is the activation energy of small polarons, and K_B denotes the Boltzmann constant. The E_p for the NMCO7 sample (as given in Table I) is inferred from the slope of ln(ρ/T) versus 1/T graph displayed in Fig. 2(b).

In Fig. 2(b) the temperature at which deviation from linearity occurs is referred to as $\frac{\theta_D}{2}$ (where $\boldsymbol{\theta_D}$ denotes Debye temperature).[24] To assess if the polaron conduction is adiabatic or non-adiabatic, we applied Holstein's conduction criterion. This criterion specifies that the polaron bandwidth (J) must satisfy specific conditions.[24,26]

$$J > \varphi \quad \text{or} \quad \frac{J}{\varphi} > 1 \quad \text{(for adiabatic hopping)}$$

$$J < \varphi \quad \text{or} \quad \frac{J}{\varphi} < 1 \quad \text{(for non-adiabatic hopping)}$$

where J and φ are calculated using the following relations:[24,26]

$$J \cong 0.67 h\nu_{ph}\left(\frac{T}{\theta_D}\right)^{\frac{1}{4}} \tag{3}$$

$$\varphi = \left(\frac{2k_B T E_p}{\pi}\right)\left(\frac{h\nu_{ph}}{\pi}\right)^{\frac{1}{2}} \tag{4}$$

in which $\boldsymbol{\nu_{ph}}$ (optical phonon frequency) is computed using the following expression.[24,26,27]

$$\nu_{ph} = \frac{k_B \theta_D}{h} \tag{5}$$

Using the above equations, we can formulate the following relation:

$$\frac{\boldsymbol{J}}{\boldsymbol{\varphi}} = 1.33\left(\frac{\boldsymbol{k_B \theta_D}}{\boldsymbol{E_p}}\right)^{\frac{1}{4}} \tag{6}$$

Table I shows that the value of $\frac{J}{\varphi}$ is less than 1, indicating that the conduction in the sample being studied is determined by non-adiabatic small polaron hopping. As noted by Austin and Mott, $\boldsymbol{\gamma_p}$(e-ph coupling parameter) offers insight into the strength of e-ph interactions and is defined by the relation given in Eq. (7).[24,26]

$$\gamma_p = \frac{2E_p}{h\nu_{ph}} \tag{7}$$

For $\gamma_p > 4$ strong e-ph interactions are indicated within the system, whereas a value <4 suggests weak interactions. The values of ν_{ph}

and γ_p are provided in Table I and for NMCO7 sample $\gamma_p > 4$, reflecting significant electron–phonon interactions in this material. The strong electron–phonon coupling leads to charge carrier localization. The Jahn–Teller distortion from Mn^{3+} ions[20] further localizes carriers, hindering the hopping process via the double-exchange mechanism. It also alters the Mn–O–Co or Co–O–Co superexchange angle and bond length, driving the overlap of O(2p) and (Mn, Co) (3d) bands, which controls the opening and closing of the charge transfer gap.

At low temperatures, the thermal activation and SPH models are typically not applicable. Consequently, to examine the impact of disorder-induced localization of charge carriers on electrical transport properties, the resistivity data as a function of temperature was analyzed employing the VRH model, as described below.[28,29] The variable range hopping model posits that charge transport in semiconductors occurs not through conventional band transport, but rather through "jumps" between localized states.[16] VRH model (Mott-type) is described by

$$\rho = \rho_0 e^{\left(\frac{T_o}{T}\right)^{\frac{1}{4}}} \tag{8}$$

Where the characteristic temperature (T_o) can be expressed as

$$T_o = \frac{18}{K_B \alpha^3 n(E_F)} \tag{9}$$

Here K_B, α, and $n(E_F)$ represent Boltzmann's constant, localization length, and the density of states at the Fermi level respectively. At a particular temperature, the hopping energy, $E_h(T)$, and hopping distance, $R_h(T)$, are defined as.[28]

$$E_h(T) = \left(\frac{1}{4}\right) k_B T^{\frac{3}{4}} T_o^{\frac{1}{4}} \tag{10}$$

$$R_h(T) = \left(\frac{3}{8}\right) \alpha \left(\frac{T_o}{T}\right)^{\frac{1}{4}} \tag{11}$$

The resistivity data for NMCO7, as presented in Fig. 2(c) and analyzed using Eq. (8), indicates a good agreement with Mott-VRH. This implies that the conduction mechanism is governed by charge carrier localization, which arises from disorder in the material.[28] This disorder originates from the presence of mixed valent Mn and Co ions[20] that induce distortion in the NMCO7 sample. Applying the values of T_o derived from the slope of Fig. 2(c), along with the above mentioned equations, the density of states, hopping energy, and hopping distance at 300 K were calculated, assuming a localization length (α) of 4.5 Å as described by Viret *et al.*[30] (refer to Table II).

TABLE II. Transport parameters for NMCO7 sample calculated using Mott-VRH.

Sample	T_o (K)	$n(E_F)$ (eV^{-1}-m^{-3})	$E_h(T)$ (eV) at T = 300 K	$R_h(T)$ (A°) at T = 300 K
NMCO7	8.059×10^8	2.844×10^{24}	0.262	68.318

IV. CONCLUSIONS

In this study, the electrical transport phenomenon of polycrystalline $NdMn_{0.3}Co_{0.7}O_3$ sample was investigated. The sample exhibited semiconductor properties. Several theoretical models were employed to analyze the electrical resistivity behavior across different temperature regions. The results indicated that the transport mechanism is governed by thermal activation and SPH models at high temperatures; however, at low temperatures, Mott-VRH is applicable.

ACKNOWLEDGMENTS

One of the authors, Farooq H. Bhat, gratefully acknowledges the financial support from the Islamic University of Science and Technology (IUST), Kashmir, under Project Order No. IUST/Acad/RP_App/17/298, and from DST-SERB under the Core Research Grant (Project No. CRG/2022/007060). Special thanks to Dr. D. K. Shukla UGC-DAE CSR, Indore, India for extending the experimental facility to perform the resistivity measurements.

AUTHOR DECLARATIONS

Conflict of Interest

The authors have no conflicts to disclose.

Author Contributions

Farooq Hussain Bhat: Conceptualization (equal); Data curation (equal); Formal analysis (equal); Funding acquisition (equal); Investigation (equal); Methodology (equal); Project administration (equal); Resources (equal); Software (equal); Supervision (equal); Validation (equal); Writing – review & editing (equal). **Jan Asifa**: Formal analysis (equal); Software (equal); Writing – original draft (equal). **Ghazala Anjum**: Formal analysis (equal); Investigation (equal); Software (equal); Visualization (equal); Writing – review & editing (equal).

DATA AVAILABILITY

The data that support the findings of this study are available from the corresponding author upon reasonable request.

REFERENCES

[1] S. Vadnala, S. Asthana *et al.*, ISRN Mater. Sci., 728195 (2013).
[2] Y. Wang *et al.*, J. Appl. Phys. **136**, 093902 (2024).
[3] Y. Wang *et al.*, J. Appl. Phys. **132**, 183907 (2022).
[4] F. H. Bhat, G. Anjum *et al.*, Ceram. Int. **47**(5), 6753–6763 (2021).
[5] N. Adeela, U. Khan, S. Naz, M. Iqbal *et al.*, Appl. Surf. Sci. **422**, 184–191 (2017).
[6] J. Dhahri, S. Zemni, K. Cherif, J. Dhahri, M. Oumezzine, M. Ghedira, and H. Vincent, J. Alloys Compd. **394**, 51 (2005).
[7] V. Vashook, D. Franke, J. Zosel, K. Ahlborn, L. Vasylechko, W. Fichtner, and U. Guth, Solid State Ionics **179**, 135 (2008).
[8] K. Yadav, M. P. Singh, F. S. Razavi, and G. D. Varma, Mater. Sci. Eng., B **177**, 1219 (2012).

[9]Q. Q. Jiang, J. H. Tong, G. L. Zhou, Z. X. Jiang, Z. Li, and C. Li, Sol. Energy **103**, 425 (2014).
[10]A. Muñoz, J. A. Alonso, M. J. Martìnez-Lope, J. L. García-Muñoz, and M. T. Fernández-Díaz, J. Phys.: Condens. Matter **12**, 1361 (2000).
[11]T. Chatterji, B. Ouladdiaf, and D. Bhattacharya, J. Phys.: Condens. Matter **21**, 306001 (2009).
[12]F. H. Bhat and G. Anjum, AIP Adv. **14**, 025041 (2024).
[13]X. J. Fan, H. Koinuma, and T. Hasegawa, Phys. Rev. B **65**, 144401 (2002).
[14]S. Angappane, G. Rangarajan, and K. Sethupathi, J. Appl. Phys. **93**, 8334 (2003).
[15]M. H. Phan, V. Franco, N. S. Bingham, H. Srikanth, N. H. Hur, and S. C. Yu, J. Alloys Compd. **508**, 238 (2010).
[16]H. Wang *et al.*, J. Mater. Sci.: Mater. Electron. **35**, 1097 (2024).
[17]H. Wang *et al.*, J. Alloys Compd. **1008**, 176718 (2024).
[18]F. Dong *et al.*, J. Mater. Sci.: Mater. Electron. **34**, 2322 (2023).
[19]H. Zhang, Y. Wang, H. Wang, D. Huo, and W. Tan, J. Appl. Phys. **131**, 043901 (2022).
[20]F. H. Bhat *et al.*, J. Magn. Magn. Mater. **615**, 172798 (2025).
[21]A. Bhogra, A. Masarrat, R. Meena *et al.*, Sci. Rep. **9**, 14486 (2019).
[22]J. P. Palakkal, P. N. Lekshmi, S. Thomas, M. Valant, K. G. Suresh, and M. R. Varma, Mater. Res. Bull. **76**, 161 (2016).
[23]W. Khan, A. H. Naqvi *et al.*, J. Chem. Phys. **135**, 054501 (2011).
[24]F. Denbri, N. Mahamdioua *et al.*, Solid State Commun. **342**, 114614 (2022).
[25]A. E. M. A. Mohamed, A. M. Mohamed, A. ElShafaie, H. F. Mohamed, A. K. Diab, and A. M. Ahmed, Chem. Phys. Lett. **713**, 272–276 (2018).
[26]L. T. T. Ngan, N. T. Dang *et al.*, J. Alloys Compd. **911**, 164967 (2022).
[27]R. Rozilah, N. Ibrahim, Z. Mohamed, A. K. Yahya, N. A. Khan, and M. N. Khan, Physica B **521**, 281–294 (2017).
[28]F. A. Khan, M. Arshad *et al.*, J. Am. Ceram. Soc. **105**, 348–361 (2022).
[29]B. Song Yi, C. Hyunyong, and R. Jong-Soo, J. Alloys Compd. **863**, 158093 (2020).
[30]M. Viret *et al.*, Phys. Rev. B **55**, 5144 (1997).